Calculations of high-order harmonic-generation processes in xenon at 1064 nm

Anne L'Huillier and Philippe Balcou
Service des Photons, Atomes et Molécules, Centre d'Etudes de Saclay, 91191 Gif-sur-Yvette, France

Sebastien Candel
Laboratoire d'Energétique Moléculaire et Macroscopique, Combustion, Ecole Centrale Paris, Chatenay-Malabry, France

Kenneth J. Schafer and Kenneth C. Kulander
Physics Department, Lawrence Livermore National Laboratory, Livermore, California 94550
(Received 25 February 1992)

We perform detailed calculations of harmonic conversion in a 15-Torr jet of xenon into which a 1064-nm-wavelength 36-ps-pulse-width laser has been tightly focused, so that the peak intensity ranges from 5×10^{12} to 5×10^{13} W cm^{-2}. The single-atom emission rates are obtained by integrating the time-dependent Schrödinger equation. We employ an improved atomic model which includes excitation and ionization through states with both low-lying ionic cores. The propagation equations are solved using a general and efficient finite-difference technique. Excellent agreement with experimental data is obtained. We consider the effect of the defocusing of the pump beam by the free electrons in the saturation regime, and find it to be small for the conditions studied here. The spatial, temporal, and spectral profiles of the harmonic emission are presented. Significant blueshifts of the harmonics' spectral line shapes are observed in the saturation regime. Finally, using model polarizations, we discuss how the harmonic fields build up in the nonlinear medium, through a series of interferences. It allows us to understand why efficient phase matching can be achieved in a strong-field regime for the laser-atom interaction.

PACS number(s): 42.65.Ky, 32.80.Rm

I. INTRODUCTION

The theoretical description of harmonic-generation processes in gases exposed to strong laser fields involves two steps: (1) the calculation of the single-atom dipole moment, obtained by solving the Schrödinger equation for an atom in the presence of an intense electromagnetic field, and (2) the integration of the propagation equations for the harmonic fields created in the medium. The first part of the problem has been thoroughly studied in the past two years. Various methods have been used [1–10]. Kulander and co-workers [1,2], DeVries [3], and LaGattuta [4] have solved numerically the time-dependent Schrödinger equation for several atomic systems. Potvliege and Shakeshaft [5] have performed Floquet calculations for hydrogen. A number of model calculations (e.g., one-dimensional approximations) have also provided some insight into the physics of the problem [6–11].

In contrast, the second aspect of the problem is only beginning to be investigated. In the traditional (perturbative) treatment of harmonic-generation processes [12–14], one separates the calculation of the atomic dipole moment from the evaluation of propagation effects. Phase matching is generally accounted for by assuming lowest-order perturbation theory to be valid or, in the case of resonant processes, by reducing the atomic system to a few interacting (discrete) levels [12,15,16]. In these cases, the polarization induced by the laser field takes a simple analytic form and the propagation equation reduces in general to a one-dimensional integral over the nonlinear medium (called the phase-matching integral).

However, this approach is not appropriate to the recent high-order harmonic-generation experiments [17–20] which involve intense fields ($\geq10^{13}$ W cm^{-2}) and numerous resonance effects [21,22]. In such experiments, e.g., at 1064 nm with a 36-ps Nd:YAG (where YAG represents yttrium aluminum garnet) laser, the observed distribution of harmonic strengths displays a characteristic shape, with a long plateau extending from approximately the fifth harmonic to one of high order. The cutoff at the end of the plateau, which can be at a rather high frequency, depends on the laser intensity and on the atomic system. Only the lowest-order harmonics vary as I^q, where q denotes the harmonic order and I the laser intensity. The harmonics in the plateau exhibit a more complex behavior than a simple power law. On average, they vary more slowly with intensity than the qth power predicted in the weak-field limit. Therefore, the theoretical description of these experiments requires the solution of the propagation equation for a general, i.e, nonperturbative polarization field [24–26].

In a recent letter [24], we have presented calculations of harmonic generation in xenon at 1064 nm in the 10^{13}-W cm^{-2} range. The atomic dipole moment, which provides the source for the polarization field, was obtained from the numerical integration of the time-dependent Schrödinger equation for the atom. At these intensities, the single-atom emission amplitudes at the harmonic frequencies are found to depart substantially from those predicted by weak-field theories. The propagation equations

for the macroscopic harmonic fields generated in the nonlinear medium were solved in integral form. Some of the results have also been discussed in a recent review article [25]. In the present work, we give a full account of these calculations and provide detailed comparisons with experimental data. Since the earlier results presented in Refs. [24,25], the single-atom part of the calculations has been improved by accounting, within the single-active-electron approximation, for the effects due to the two spin-orbit components ($^2P_{1/2}$ and $^2P_{3/2}$) of the residual ion. In the propagation calculations, we now use more accurate parameters for the laser and interaction geometries which have been recently measured [22]. This allows us to make a more rigorous comparison between calculated and experimental values. Additionally, we employ a different, and more general, method for solving the propagation equation, based upon finite-difference techniques. Thus, we can include the modification of the fundamental field (due to a nonlinear refractive index) and study its influence (found to be weak) on the generation of the harmonic fields. Moreover, we can determine the fields everywhere, including within the medium itself. Applying this method to model polarization fields provides us with a clearer physical interpretation of why efficient phase matching is achieved in strong laser fields. In the weak-field, perturbative limit, very few photons actually get out of the medium because the polarization field is very strongly peaked at the point of maximum pump intensity so that the generated harmonic field first increases to a maximum and then decreases before reaching the edge of the medium. In the strong-field regime, the polarization varies much less rapidly with intensity. Phase-matching oscillations owing to constructive and destructive interferences in the medium appear. Simultaneously, the harmonic field becomes defocused and develops rings which can propagate to the boundary of the gas. As a result, the field that exits the medium can be much more intense than in the perturbative limit.

This article is organized as follows: In Sec. II we describe the details of our theoretical approach. Comparisons with experimental data are presented in Sec. III. Finally, we discuss the difference between phase matching in weak and in strong laser fields in Sec. IV.

II. THEORETICAL METHOD

A. Propagation equations

We give here only the essential equations needed to understand the calculations presented in Sec. III and refer the reader interested in more details about the derivation of these equations to the review articles [20] and [25]. We start from the propagation equation for the qth harmonic field $\mathcal{E}_q$, obtained by Fourier transforming the time-dependent propagation equation

$$\nabla^2\mathcal{E}_q+(n_q q\omega/c)^2\mathcal{E}_q=-4\pi(q\omega/c)^2\mathcal{P}_q \ . \tag{1}$$

ω is the laser frequency, c the speed of light, and n_q the refractive index of the medium. $\mathcal{P}_q$ is the polarization induced by the fundamental field only; we can neglect the influence of wave-mixing processes involving other (lower-order) harmonic fields and the depletion of the fundamental field. In the weak-field limit, the refractive index n_q is defined by

$$n_q(z)=1+2\pi\mathcal{N}(z)\chi^{(1)}(q\omega) \ , \tag{2}$$

where $\chi^{(1)}(q\omega)$ is the atomic dipole polarizability. The refractive index $n_q(z)$ is z dependent if the medium density $\mathcal{N}(z)$ changes along the z axis (propagation axis). We consider a nonlinear medium uniform in the direction perpendicular to the laser axis (in the absence of ionization). In strong laser fields such that (single) ionization becomes significant, the refractive index will include contributions from the populations of ions and electrons:

$$\begin{aligned} n_q(\mathbf{r},z)=1&+2\pi\mathcal{N}_a(\mathbf{r},z)\chi_a^{(1)}(q\omega,|\mathcal{E}_1|^2) \\ &+2\pi\mathcal{N}_i(\mathbf{r},z)\chi_i^{(1)}(q\omega,|\mathcal{E}_1|^2) \\ &+2\pi\mathcal{N}_e(\mathbf{r},z)\chi_e^{(1)}(q\omega) \ , \end{aligned} \tag{3}$$

where the indices a, i, or e refer to the atomic, ionic, or electronic density or polarizability. Note that $n_q(\mathbf{r},z)\approx 1$ so that the spatial variation of the index needs to be accounted for only when differences between indices are involved. The notation $\chi^{(1)}(q\omega,|\mathcal{E}_1|^2)$ implies that, for an atomic or ionic system exposed to a strong laser field, the polarizability becomes dependent on the intensity of the fundamental field ($|\mathcal{E}_1|^2$). For a free electron, it reduces simply to $-e^2/mq^2\omega^2$, where e and m are the charge and mass of the electron. In our calculations, we neglect the contribution from ions to the polarizability (refractive index) and to the laser-induced polarization $\mathcal{P}_q$. The contribution from free electrons is included and it is assumed that the electron density remains equal to the ion density, an approximation which is valid for short laser pulses. Thus, the propagation problem is axisymmetric and may be expressed in terms of (r,z) cylindrical coordinates.

First, we consider the case where the refractive index n_q depends only on the z coordinate. We introduce the envelope functions

$$E_q=\mathcal{E}_q\exp\left[-i\int_{-\infty}^{z}k_q(z')dz'\right]$$

and

$$P_q=\mathcal{P}_q\exp\left[-i\int_{-\infty}^{z}qk_1(z')dz'\right]$$

with $k_q(z)=n_q(z)q\omega/c$ ($k_q\approx qk_1\approx q\omega/c$). In the paraxial approximation (i.e., assuming that the wave fields propagate close to the laser axis), the wave envelopes may be assumed to vary slowly in the z direction ($\partial/\partial z\ll k_q$), so that Eq. (1) becomes

$$\begin{aligned} \nabla_\perp^2E_q+2ik_q\frac{\partial E_q}{\partial z} \\ =-4\pi(q\omega/c)^2P_q\exp\left[-i\int_{-\infty}^{z}\Delta k_q(z')dz'\right] \ , \end{aligned} \tag{4}$$

where $\nabla_\perp$ acts on the transverse coordinate and $\Delta k_q=k_q-qk_1$. Note that when the refractive index n_q is complex (i.e., when the medium is absorbing at frequency $q\omega$),

$$|E_q(r,z)|^2=|\mathcal{E}_q(r,z)|^2\exp\left[2\int_{-\infty}^{z}\kappa_q(z')dz'\right],$$

where κ_q is the absorption coefficient at frequency $q\omega$ (imaginary part of k_q). Introducing

$$\tilde{E}_q=E_q\exp\left[i\int_{-\infty}^{z}\Delta k_q(z')dz'\right],$$

Eq. (4) becomes

$$\nabla_\perp^2\tilde{E}_q+2ik_q\frac{\partial\tilde{E}_q}{\partial z}+2k_q\Delta k_q\tilde{E}_q=-4\pi(q\omega/c)^2P_q\ . \tag{5}$$

In this case, $|\tilde{E}_q|^2=|\mathcal{E}_q|^2$.

We introduce r-dependent refractive indices into these equations by defining

$$k_q(r,z)=n_q(r,z)q\omega/c=k_q^0(z)+\delta k_q(r,z)\ ,$$

with

$$k_q^0(z)=(q\omega/c)[1+2\pi\mathcal{N}(z)\chi_a^{(1)}(q\omega)]\ ,$$

$\mathcal{N}(z)$ being the (initial) medium density. The slowly-varying-envelope approximation is made as before, by separating out the wave vectors $k_q^0(z)$ and $k_1^0(z)$, involving the rapid variation of the fields, and r-dependent corrections $\delta k_q(r,z)$ and $\delta k_1(r,z)$, assumed to induce slowly-varying corrections to the harmonic and fundamental fields. The propagation equations for the fundamental and incident laser fields become

$$\nabla_\perp^2E_1+2ik_1^0\frac{\partial E_1}{\partial z}+2k_1^0\delta k_1E_1=0\ , \tag{6}$$

$$\nabla_\perp^2E_q+2ik_q^0\frac{\partial E_q}{\partial z}+2k_q^0\delta k_qE_q=-4\pi(q\omega/c)^2P_q\exp\left[-i\int_{-\infty}^{z}\Delta k_q^0(z')dz'\right]. \tag{7}$$

As before, defining

$$\tilde{E}_q=E_q\exp\left[i\int_{-\infty}^{z}\Delta k_q^0(z')dz'\right],$$

Eq. (7) can be written as

$$\nabla_\perp^2\tilde{E}_q+2ik_q^0\frac{\partial\tilde{E}_q}{\partial z}+2k_q^0(\delta k_q+\Delta k_q^0)\tilde{E}_q=-4\pi(q\omega/c)^2P_q\ . \tag{8}$$

A proper treatment of the influence of intensity-dependent refractive indices (and, in particular, those induced by the presence of free electrons) requires first the solution of Eq. (6), which is nonlinear because $\delta k_1(r,z)$ depends on the field E_1. For low frequencies, pressures above 10 Torr, and intensities high enough to partially ionize the medium, the refractive index will be dominated by the free-electron contribution. Consequently, the fundamental beam will become slightly defocused as it propagates through the medium. This is because the refractive index due to free electrons is much smaller close to the propagation axis than far from it; the nonlinear medium acts as a diverging lens. Next, one calculates the nonlinear polarization P_q and the intensity-dependent wave vector $\delta k_q(r,z)$ induced by the *perturbed* fundamental field E_1. Then Eq. (7) or (8) can be solved.

Alternatively, we can choose to make the slowly-varying-envelope approximation by including in the phase term the total wave vector $k_q(r,z)$. We get

$$\nabla_\perp^2E_1+2ik_1\frac{\partial E_1}{\partial z}+2i\left[\int\frac{\partial k_1}{\partial r}dz\right]\frac{\partial E_1}{\partial r}+i\left[\int\nabla_\perp^2k_1dz\right]E_1-\left[\int\frac{\partial k_1}{\partial r}dz\right]^2E_1=0\ , \tag{9}$$

$$\nabla_\perp^2E_q+2ik_q\frac{\partial E_q}{\partial z}+2i\left[\int\frac{\partial k_q}{\partial r}dz\right]\frac{\partial E_q}{\partial r}+i\left[\int\nabla_\perp^2k_qdz\right]E_q-\left[\int\frac{\partial k_q}{\partial r}dz\right]^2E_q=-4\pi(q\omega/c)^2P_q\exp\left[-i\int\Delta k_qdz\right]. \tag{10}$$

Albeit written in a more complicated form, these equations are equivalent to Eqs. (6) and (7). Now the effect of the transverse variation of the refractive index and the change in the phase mismatch between the generated and driving field are clearly distinguished. If one neglects the transverse variation of the refractive index, which implies that the fundamental field does not get defocused as it propagates through the nonlinear medium, Eq. (10) reduces to an equation identical to Eq. (4) (except that the wave-vector mismatch Δk_q now depends on the transverse coordinate r) or to Eq. (5), with the additional transformation from E_q to $\tilde{E}_q$.

In previous articles [24,25], we have presented results obtained by neglecting the modification of the fundamental field and by calculating the far-field envelope expressed in integral form [see, e.g., Eq. (3.16) in [25]]. In the present work, the propagation equations are solved numerically over the length of the nonlinear medium by using finite-difference techniques. As will be shown later, this gives additional insight into the physics of the problem because it shows the variation of $E_q(r,z)$ as it is generated in the nonlinear medium. It also allows us to include the defocusing of the fundamental field, though, as will be shown later, this effect remains weak (negligible) in the conditions studied here. The propagation equations are discretized in the (r,z) plane on a 500×300 point grid and integrated using a space-marching Crank-Nicholson scheme. The field at the position z_i is obtained from that at the position z_{i-1} by inverting a tridiagonal matrix with a classical recursive algorithm.

All of the above variable (fields, wave vectors, and densities) should be understood to be slowly time varying because the incident laser field is a pulse. The propagation equations are solved for a sequence of times t spanning the pulse duration. The number of harmonic photons N_q emitted at each laser pulse is then obtained by integrating $|E_q(r,z,t)|^2$ in space and time:

$$N_q=\frac{c}{4\hbar q\omega}\int|E_q(r,z,t)|^2r\,dr\,dt\ . \tag{11}$$

This integral is independent of the position z on the propagation axis, as long as z is outside the medium

In Sec. II B we discuss how the different components of the propagation equations are determined. We first consider the single-atom part of the calculations.

B. Single-atom response

In these calculations, we need to determine (1) the harmonic components of the laser-induced dipole moment $d(t)$, i.e., the sources of harmonic radiation; (2) the ionization rate that allows us to follow the atomic (electronic) density in the medium and consequently to evaluate the phase mismatch due to free electrons; and (3) the dipole polarizability at the fundamental and harmonic frequencies from which we determine the phase mismatch due to the neutral atoms.

Most of the calculations of these single-atom components to the macroscopic harmonic emission rates have been carried out using our single-active-electron (SAE) model. In this model we hold the orbitals of all but one of the electrons in the atom fixed and allow the active electron to respond to the laser in the mean field of the nucleus and remaining electrons. We solve the time-dependent Schrödinger equation for this electron in a laser which turns on to its maximum intensity over five optical cycles and then has a constant intensity for the next 20–30 cycles. After the ramp, the transient excitations decay by ionization over the next few cycles. The ionization rate and photoemission rates are determined, for the particular fixed intensity and wavelength, during the last part of the pulse. The details of these calculations have been presented elsewhere [27] and are repeated here only to the extent necessary to describe an improvement we have made in the SAE model. Because the harmonic-generation experiments are carried out in rare gases, some accommodation for the existence of a second, low-lying ionization limit in these species has been made. In the past we had considered only ionization into the lowest continuum. For the wavelengths and intensities used in the experiments, ionization and, in particular, excitation into the manifold of states converging to the second ionization limit have been observed to be significant, especially in the lighter rare-gas species. Moreover, it is important to account for the correct orbital occupancy of the active electron responsible for the emission.

The effective potentials for the electron are generated according to the description given previously in [27,28]. The potentials are constructed from the valence orbitals of the atom. We carry out Hartree-Slater calculations on the ground and singly excited states of the atom, adjusting the exchange-correlation parameter so that the orbital energy of interest agrees with the spectroscopic value. The valence orbital, which has a particular value of the orbital angular momentum, l, is then used to construct an l-dependent effective potential whose lowest eigenvalue is the ionization energy of that state. This procedure is repeated for different l values to generate the complete potential. We use the $l=2$ potential for $l \geq 2$. This method results in quite accurate excitation energies, much better than normally obtained in either Hartree-Fock or Hartree-Slater calculations. However, it provides a model of the xenon atom which accounts only for the manifold of singly excited states based on the lowest ionic core $^2P_{3/2}$. For all rare gases, a second manifold of states converges to the next spin component of the ion, the $^2P_{1/2}$ state. Therefore, we repeat the above procedure to obtain effective potentials for this second set of excited states. We assume that these two manifolds are very weakly coupled through multiphoton excitation so that they can be treated separately. This assumption is reasonable because once one of the electrons is excited, leaving a particular core state, transitions into states with the other core would require a two-electron transition. Thus it is within the spirit of the SAE approximation to neglect such excitation pathways. The contributions to the induced dipole responsible for the harmonics from these separate calculations are added coherently.

In xenon the splitting between the ion core limits is quite large, approximately 1.3 eV, slightly more than the photon energies considered in this work. We find the contributions from this second manifold are not too significant for the range of intensities studied here. However, for shorter laser pulses and for the lighter rare gases, the atom can experience higher laser intensities, and the contributions from these additional excited states will become relatively more important and even sometimes dominant.

An important effect due to the spin-orbit coupling, however, does come into play even though the upper ionic core is not specifically involved. This is because the excitation dynamics is very sensitive not only to the ionization potential or binding energy of the active electron but also to m, the projection of the orbital angular momentum along the polarization axis [28]. The valence shell p electrons in xenon with $m=0$ are found to provide the dominant contribution to the high-order harmonic emission by the atom. Since no spin-orbit terms are included in our Hamiltonian explicitly, we solve the Schrödinger equation in LS coupling. This means that for a linearly polarized laser field, m is a good quantum number. Therefore, we need to assign the weights to the valence orbitals according to their weights in the spin-orbit-coupled states. There are two $m=0$ valence electrons in the p shell, $\frac{4}{3}$ associated with the $^2P_{3/2}$ core and $\frac{2}{3}$ with $^2P_{1/2}$. Contributions from the other four p electrons which have $|m|=1$ to the harmonic-emission strengths are found to be unimportant for the intensities considered here. Therefore, we solve the time-dependent Schrödinger equation for the $\frac{4}{3}$ electrons with $m=0$, which leave the ion in the $^2P_{3/2}$ core state, and for the $\frac{2}{3}$ electrons with $m=0$, which leave the ion in the $^2P_{1/2}$ core state. The emission strengths at the harmonic frequencies are then obtained from the Fourier transform of the total induced dipole calculated over the period of the last five cycles of the pulse described above:

$$d_q = \frac{1}{T_2 - T_1} \int_{T_1}^{T_2} e^{iq\omega t} \langle \Psi(t)|z|\Psi(t)\rangle dt \ . \tag{12}$$

We obtain the ionization rate for each intensity by

monitoring the norm of the wave function during the constant-intensity interval. Our finite-difference calculations are performed in a finite box with absorbing boundaries. As flux reaches the edges of the grid, it is removed. We define the rate at which this occurs to be the ionization rate.

Finally, the last atomic quantity we need is the dipole polarizability $\chi_a^{(1)}(q\omega,|\mathcal{E}_1|^2)$. Here, we have preferred to depart from the single-active-electron approximation. Indeed, though this approximation is good for low excitation frequencies and high laser intensities, it cannot describe sufficiently accurately the photoabsorption cross section over a large energy range [29]. The solution of the three-dimensional Schrödinger equation for several active electrons in the presence of a strong laser field remains unfortunately beyond reach at present, and we have simply calculated the dipole polarizability to lowest order in the radiation field [$\chi_a^{(1)}(q\omega)$], using a many-body perturbation-theory approach [30].

In fact, we also tried to estimate the magnitude of intensity-dependent corrections to the zero-order atomic polarizability at harmonic frequencies close to the ionization threshold and its influence on the macroscopic harmonic-emission rates. This has been done by using a crude, modified perturbative model, including a few discrete excited states only, whose energies have been assumed to shift with the laser field as the ponderomotive energy. We find that by the time the field strength is high enough that $\chi_a^{(1)}(q\omega,|\mathcal{E}_1|^2)$ begins to differ from its weak-field limit, the ionization probability becomes important. Then the nonlinear refractive indices are dominated by the contribution from free electrons. Moreover, the neutral-atom population (the source of the harmonic emission) is depleted. Consequently, the emission rates are found to be only weakly affected by these intensity-dependent corrections. They will not be included in the results presented below.

C. Polarization and phase mismatch

We now relate the single-atom components introduced in Sec. II B to the macroscopic variables involved in the propagation equations: the laser-induced nonlinear polarization P_q; the r-dependent corrections to the wave vectors $\delta k_1,\delta k_q$ [Eqs. (6) and (7)]; and the phase mismatch Δk_q [Eq. (5)]. The polarization $P_q(r,z,t)$ is defined by

$$P_q(r,z,t)=2\mathcal{N}_a(r,z,t)d_q(r,z,t)\times\exp\left[-iq\left[\tan^{-1}(2z/b)-\frac{2k_1r^2z}{b^2+4z^2}\right]\right], \tag{13}$$

where $d_q(r,z,t)$ is the component of the atomic dipole moment oscillating at frequency $q\omega$ calculated for the field strength $|E_1(r,z,t)|$. The factors of 2 arises from the different conventions used in the definition of P_q [the total polarization $\mathcal{P}(t)$ is decomposed as $\sum_q \mathcal{P}_q e^{iq\omega t}/2+\text{c.c.}$] and in the definition of d_q as the Fourier transform of $d(t)$. The phase factor in Eq. (13) (see [25] for more details) comes from the fact that the Schrödinger equation is solved for a real field [$|E_1|\sin(\omega t)$], whereas the equations of propagation for focused beams involve complex amplitude wave fields. Here, we have expressed the polarization induced by an incident Gaussian field, not modified as it propagates in the medium. Its envelope $E_1(r,z,t)$ is given by

$$E_1(r,z,t)=\frac{bE_0}{b+2iz}\exp\left[-\frac{k_1r^2}{b+2iz}\right]\times\exp[-2\ln(2)(t/\tau)^2], \tag{14}$$

where τ is the pulse full width at half maximum, b the laser confocal parameter, and E_0 the peak field strength. It is of interest to separate out the phase and the amplitude of E_1 as

$$E_1(r,z,t)=\frac{bE_0}{(b^2+4z^2)^{1/2}}\exp\left[-\frac{k_1r^2b}{b^2+4z^2}\right]\exp[-2\ln(2)(t/\tau)^2]\exp\left[-i\left[\tan^{-1}(2z/b)-\frac{2k_1r^2z}{b^2+4z^2}\right]\right]. \tag{15}$$

The phase factor in Eq. (13) is simply q times the Gaussian beam phase [Eq. (15)]. More generally, it is q times the phase of the fundamental field in the medium. Finally, the atomic density $\mathcal{N}_a(r,z,t)$ is defined by

$$\mathcal{N}_a(r,z,t)=\mathcal{N}(z)\exp\left[-\int_{-\infty}^{t}p(r,z,t')dt'\right], \tag{16}$$

where $p(r,z,t')$ is the ionization rate calculated at the field strength $|E_1(r,z,t')|$. We assume that the gas jet density distribution is a truncated Lorentzian function $\mathcal{N}(z)=\mathcal{N}_0\rho(z)$, where $\mathcal{N}_0$ is the initial peak density and where $\rho(z)$, the (normalized) atomic profile, is given by $\rho(z)=1/(1+4z^2/L^2)$ for $|z|\le L$, $=0$ elsewhere.

The phase mismatch $\Delta k_q(r,z,t)$ is approximated by the sum of the atomic phase mismatch (to lowest order in the radiation field) and the contribution from the free electrons, which becomes important when the medium begins to ionize:

$$\Delta k_q(r,z,t)=2\pi(q\omega/c)\mathcal{N}_a(r,z,t)[\chi_a^{(1)}(q\omega)-\chi_a^{(1)}(\omega)]+\frac{2\pi(q^2-1)e^2}{mcq\omega}[\mathcal{N}(z)-\mathcal{N}_a(r,z,t)]. \tag{17}$$

Similarly, we have ($q\ge 1$)

$$\delta k_q(r,z,t)=2\pi(q\omega/c)[\mathcal{N}_a(r,z,t)-\mathcal{N}(z)]\chi_a^{(1)}(q\omega)-\frac{2\pi e^2}{mcq\omega}[\mathcal{N}(z)-\mathcal{N}_a(r,z,t)]. \tag{18}$$

III. RESULTS AND COMPARISON WITH EXPERIMENTAL DATA

The calculations have been performed for xenon at 1064 nm in the 5×10^{12}–5×10^{13}-W cm^{-2} intensity range. The macroscopic parameters in the calculations (focusing conditions and atomic beam geometry) have been chosen to mimic the experimental conditions as closely as possible. The atomic density distribution follows a Lorentzian profile with a full width at half maximum $L=0.8$ mm and a total width of $2L$ [22]. The peak atomic density is 15 Torr (5.3×10^{17} atoms/cm^3). The laser confocal parameter b has been recently measured to be ≈1.5 mm. Finally, the laser pulse width is 36 psec.

First we show the effect of the nonlinear refractive index induced by the free electrons on the propagation of the fundamental beam. The profile of the incident field at the far edge of the medium (at 0.8 mm from the focus) is shown in Fig. 1(a). The solid line indicates the profile in the weak-field limit, i.e., not modified by the interaction with the nonlinear medium. The dot-dashed line presents the fundamental field which has been defocused by the nonuniform electron density created at 4.9×10^{13} W cm^{-2} (our highest laser intensity). The curves, normalized to have the same maximum value, correspond to the near-field profile integrated over the pulse width. One sees that the defocusing of the fundamental field remains weak for the conditions studied here. It will be neglected in most of the calculations presented below. Indeed, this approximation allows us to solve only one propagation equation [Eq. (5)] instead of two coupled ones [Eqs. (6) and (8)]. It is also of interest to examine how the line shape of the fundamental beam is modified by the interaction. Figure 1(b) shows the spectral profile calculated by Fourier transforming the pulse amplitude at the far edge of the medium. The free electrons induce an additional time-dependent phase factor,

$$\delta\Phi(t)=-\int_{-\infty}^{z}\delta k_1(z,t)dz\ ,$$

which results in a (small) blueshift ($\delta\omega=\delta\Phi/\delta t\geq0$) of the spectral line shape. These effects induced by the free electrons will become much more important at higher pressures [31,32].

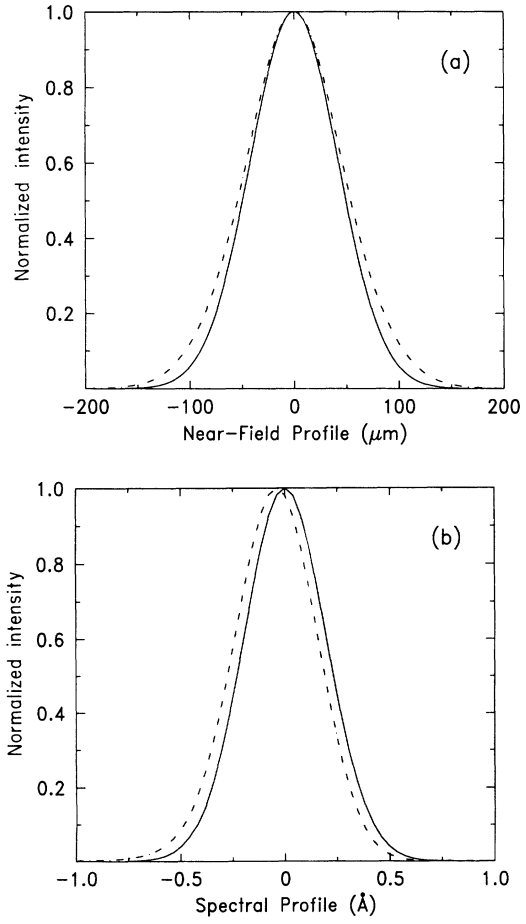

FIG. 1. Normalized (a) near-field and (b) spectral profiles of the fundamental beam, propagating in vacuum (solid line) and in a 15-Torr gas jet at 4.9×10^{13} W cm^{-2} (dot-dashed line).

Figure 2 shows the number of photons obtained in xenon at the different harmonic frequencies for the intensities 10^{13}, 1.3×10^{13}, 2×10^{13}, and 4×10^{13} W cm^{-2} from the bottom to the top. The solid circles correspond to results of calculations. The experimental data (determined to within one order of magnitude) are shown by the open squares [23]. The agreement between the experiment and our *ab initio* calculations is excellent. The main discrepancies are for the 7th and 9th harmonics at the highest intensities (2×10^{13} and 4×10^{13} W cm^{-2}).

A more detailed comparison can be made by studying the intensity dependence of the number of photons measured and calculated for each harmonic. Figures 3–7 display the results for the 3rd to the 21st harmonics. The experimental values [23] are indicated by the open circles, while the results of calculations are plotted as the solid lines. The agreement is in general very good for the intensity region below the saturation intensity (about 2.5×10^{13} W cm^{-2}), at which the ionization of the medium becomes important. Above this intensity, depletion

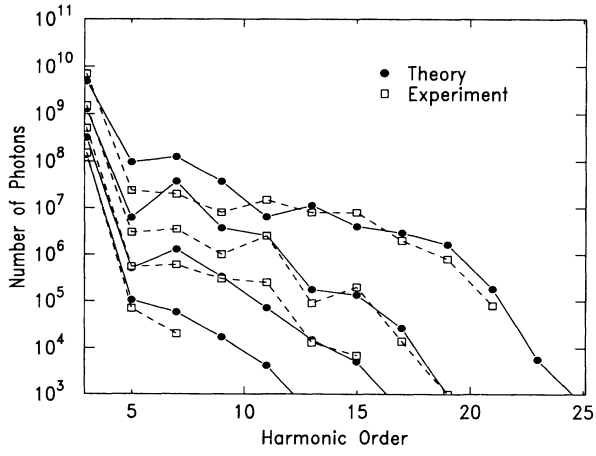

FIG. 2. Calculated (solid circles) and experimental (open squares) number of photons as a function of the harmonic order q at several intensities 10^{13}, 1.3×10^{13}, 2×10^{13}, and 4×10^{13} W cm^{-2} from the bottom to the top.

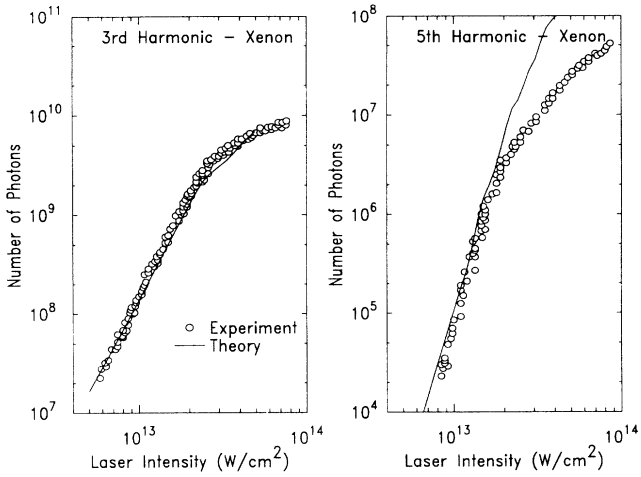

FIG. 3. Calculated (solid line) and experimental (open circles) 3rd and 5th harmonics as a function of the laser intensity.

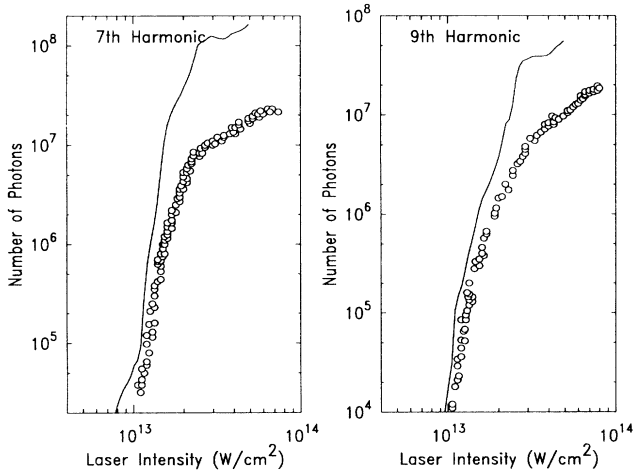

FIG. 4. Same as in Fig. 3; 7th and 9th harmonics.

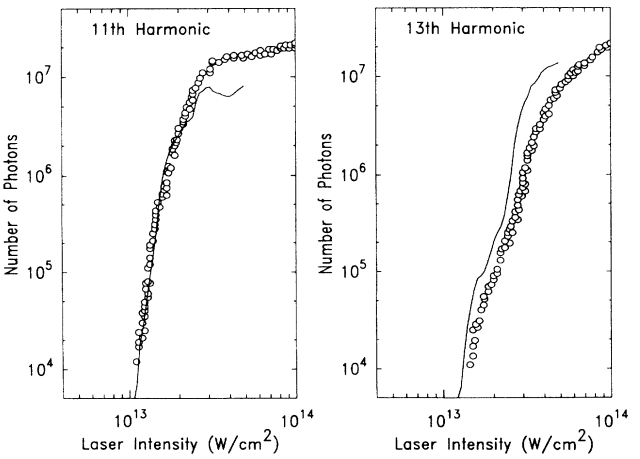

FIG. 5. Same as in Fig. 3; 11th and 13th harmonics.

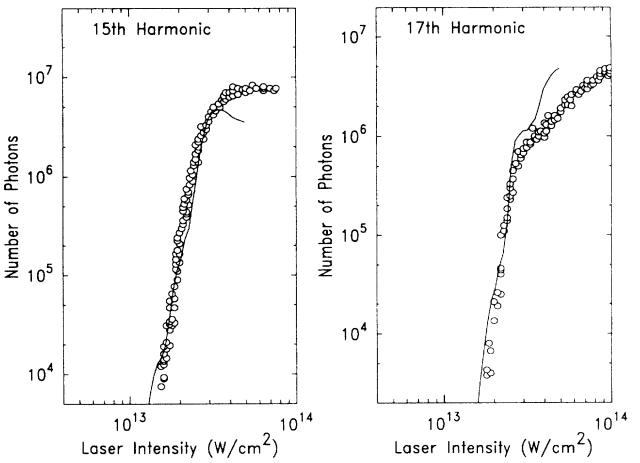

FIG. 6. Same as in Fig. 3; 15th and 17th harmonics.

of the neutral medium leads to a less rapid rise in the harmonic-conversion efficiency. Apart from the 3rd and 5th harmonics, which vary as I^3 and I^5 below saturation, all the harmonics have a more complex intensity dependence which cannot be described by a simple power law (see particularly the 7th or 13th harmonics). In general, the changes of slopes observed in the experimental data are remarkably well reproduced by the calculation. The agreement between theory and experiment is not as good in the saturation regime. The behavior above saturation seems to be strongly dependent on the harmonic order: for some of the harmonics (e.g., the 5th or the highest ones), the satuation is rather smooth, whereas for others (the 7th, the 11th, and the 15th), it is quite pronounced, sometimes displaying oscillations. The experimental data are generally smoother than the calculated results, with similar (but not identical) differences from one harmonic to the other.

In Fig. 8, we compare the number of 7th- and 13th-harmonic photons, represented by a dashed line, to the corresponding single-atom data, shown as a solid line.

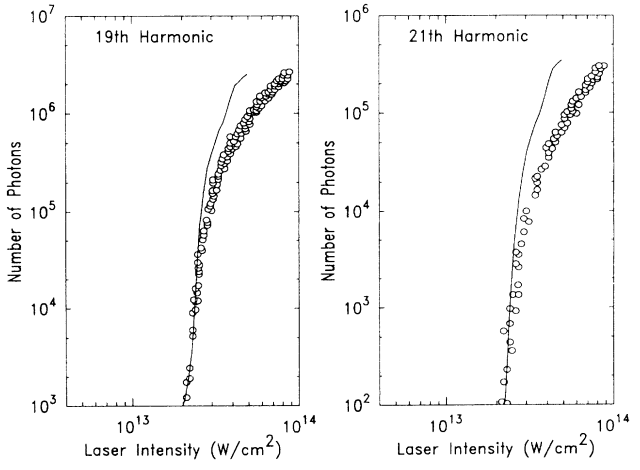

FIG. 7. Same as in Fig. 3; 19th and 21st harmonics.

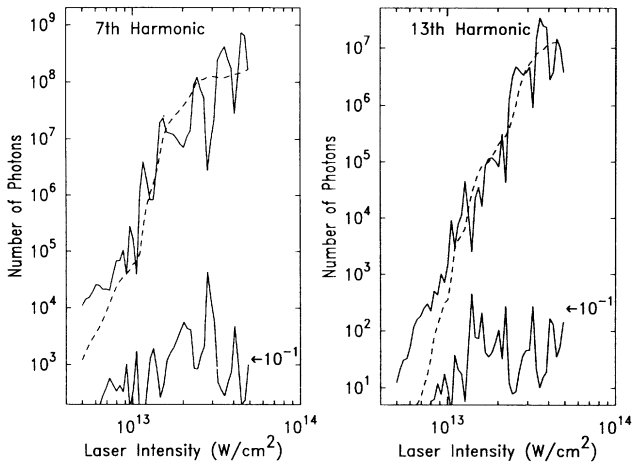

FIG. 8. Comparison between the single-atom response (solid line) and the complete calculation accounting for propagation (dashed line) for the 7th and 13th harmonics. The phase-matching factor is indicated by the solid line at the bottom.

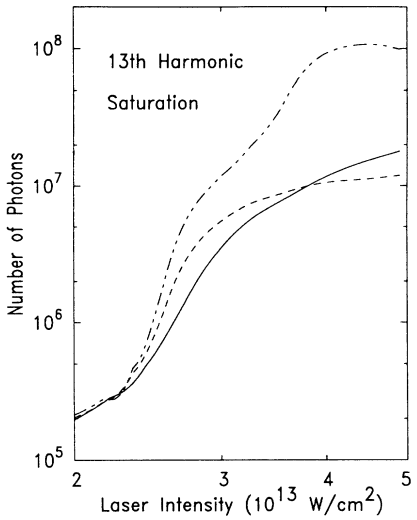

FIG. 9. 13th harmonic as a function of intensity in the saturation region calculated by using different approximations: (i) fully including the influence of the free electrons and depletion (solid line), (ii) neglecting the defocusing of the fundamental and the induced phase mismatch due to free electrons (dashed line), and (iii) neglecting also the ionization of the medium (dot-dashed line).

The latter data have been scaled so that both results can be superposed. The inclusion of propagation effects, the volume and temporal integrations, leads to a significant averaging of all of the structures and resonances. We have represented at the bottom of the figures by a solid line the variation of the phase-matching factor defined by the ratio of the number of photons N_q to the single-atom response at the peak intensity in the focal volume. It increases as the single-atom response decreases, and vice versa. Consequently, it fills in the dips and flattens out the peaks, leading to a smoother curve for the final result (dashed line). Only the average behavior of the single-atom result survives the effects of propagation. Note, however, that this average behavior can be quite different from the perturbative I^q, or, more generally, any I^p power law. The 13th harmonic exhibits a change of slope around 2×10^{13} W cm^{-2}, which can be traced back to a deep structure in the single-atom response. Note that the phase-matching factor is constant *on average* and similar for the 7th and 13th harmonics. It is close to 10^{-1}, as shown on the right side of the figures. Moreover, its average value is approximately the same for all the harmonics. This means that under these conditions the characteristic shape of the harmonic distributions (the plateau and cutoff) is determined by the single-atom response and not by any macroscopic effect.

We have studied the saturation region of the 13th harmonic in more detail. Indeed, in Fig. 8 the saturation seems to also be present in the single-atom response, without invoking any macroscopic effects such as the depletion of the neutral-atom population or the influence of the free electrons. In Fig. 9 we show results obtained by fully including the influence of the free electrons and depletion [solving Eqs. (6) and (8), solid line]; by neglecting the defocusing of the fundamental and the induced phase mismatch (dashed line), and finally by neglecting also the ionization of the medium (dot-dashed line). In the conditions studied here, the most important effect is due to the depletion of the neutral-atom population, which leads to a reduction of the number of photons by about one order of magnitude at the highest laser intensity. The reason the significant phase mismatch induced by the free electrons does not have more influence on the harmonic-emission rates is simple: The population of radiating dipoles, whose collective emission would be affected by the free electrons, simultaneously becomes depleted. In other situations, e.g., when the contribution from ions to the microscopic harmonic emission comes into play in a significant manner, the influence of the free electrons might be more important.

Finally, we have studied the spatial, temporal, and spectral profiles of the harmonics to characterize further the radiation emitted under these experimental conditions. We show in Fig. 10 the profiles of the 13th harmonic at three intensities 5×10^{12} (perturbative limit), 2×10^{13}, and 4×10^{13} W cm^{-2}. All the curves have been normalized to have the same maximum value. The near-field profile (at the far edge of the medium, i.e., at 0.8 mm from the focus) is shown in Fig. 10(a). Figure 10(b) displays the far-field profile (in radians) calculated at 30 cm from the focus. It can be obtained from the field in the near zone through a Hankel transformation [33]:

$$E_q(r',z')=-ik_q\int\frac{E_q(r,z)}{z'-z}J_0\left[\frac{k_q r r'}{z'-z}\right]\times\exp\left[\frac{ik_q(r^2+r'^2)}{2(z'-z)}\right]r\,dr\ . \quad (19)$$

where J_0 is the zero-order Bessel function. Both spatial profiles have been time integrated over the pulse width. Finally, Figs. 10(c) and 10(d) show, respectively, the temporal profile and spectral line shape of the 13th harmonic outside the medium. The harmonics are defocused com-

pared to that expected in the weak-field limit. They exhibit some structures (rings), which will be discussed in Sec. IV. Note that using a weaker focusing geometry leads to smoother (more coherent) spatial profiles. In the same way, the temporal profiles are not always regular, displaying structures which are due in part to resonance effects in the single-atom response. Ionization leads to an asymmetry in the profiles, as seen in particular in the result at 4×10^{13} W cm^{-2} [34]. The depletion and therefore the asymmetry is more significant for higher intensities. Finally, the spectral line shapes exhibit a significant shift to higher frequencies at intensities high enough to begin to ionize the medium [35]. This blueshift is induced by the fundamental blueshift and is roughly equal to q times that of the fundamental. At high intensities, the 13th-harmonic line shape broadens and shifts compared to the perturbative limit. However, it remains quite narrow, with a $\Delta\lambda/\lambda$ less than 10^{-4}. A discussion of the spatial and temporal coherence of the high harmonics generated from a more powerful, less tightly focused laser with shorter pulse duration (these characteristics are more highly optimized for harmonic emission in the extreme ultraviolet range) will be presented in a forthcoming article.

IV. DISCUSSION

In this section we discuss in detail how harmonic fields are generated in a nonlinear medium of finite length (L). Our analysis is based on three-dimensional pictures showing the amplitudes of either the polarization field $|P_q(r,z)|$ or the harmonic field $|E_q(r,z)|$, produced in the nonlinear medium at the maximum of the laser pulse ($t=0$). For the sake of a clearer presentation, we use in this section a uniform nonlinear medium rather than the Lorentzian distribution employed previously. The length of the medium is chosen to be the same as that in Sec. III. Examples of results obtained with a nonconstant density distribution have been shown in [36]. Indeed, the use of a Lorentzian medium dampens the harmonic field at its edges, making the illustration of interference effects we wish to emphasize less clear. Finally, we use a constant phase mismatch Δk_q, usually set to zero, in the cases studied below.

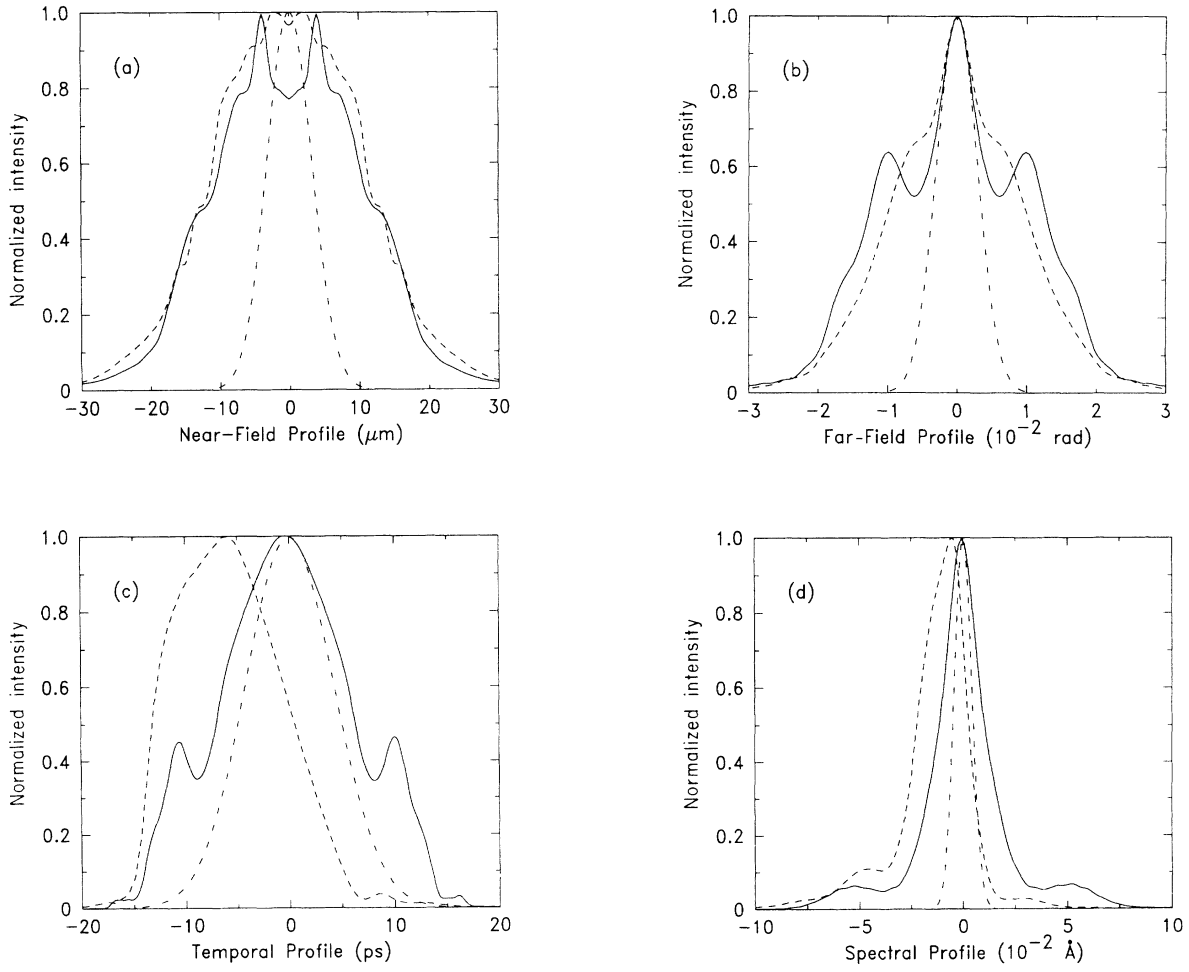

FIG. 10. Normalized 13th-harmonic profiles for several intensities: 5×10^{12} W cm^{-2} (perturbative limit, dot-dashed line), 2×10^{13} W cm^{-2} (solid line), and 4×10^{13} W cm^{-2} (dashed line). (a) Near field; (b) far field; (c) temporal; (d) spectral.

A. Weak-field limit

First we will discuss examples of perturbative harmonic generation for the 3rd, 7th, and 13th harmonics with phase mismatch of zero (Fig. 11). In the perturbative limit, the polarization field for the qth harmonic can be written as

$$P_q(r,z)=\mathcal{N}_0\chi^{(q)}E_1^q(r,z)/2^{q-1} ,$$

where $\chi^{(q)}$ denotes the qth-order nonlinear susceptibility. The incident field $E_1(r,z)$, assumed to be a Gaussian beam, is written as $E_1(r,z)=E_0G_b^{\omega}(r,z)$, where $G_b^{\omega}(r,z)$ is the envelope function

$$(1+2iz/b)^{-1}\exp[-k_1r^2/(b+2iz)] .$$

The solution of the propagation equation is given by

$$E_q(r',z')=g_qG_b^{q\omega}(r',z')\int_{-L/2}^{z'}\exp[-i\Delta k_qz-i(q-1)\tan^{-1}(2z/b)](1+4z^2/b^2)^{(1-q)/2}dz , \tag{20}$$

where

$$g_q=-i\pi k_q\chi^{(q)}2^{2-q}E_0^q .$$

The harmonic profile remains Gaussian inside and outside the medium. How the field is created and destroyed in the medium is governed by the phase-matching integral at the right side of Eq. (20). The integrand consists of an oscillatory function

$$\exp[-i\Delta k_qz-i(q-1)\tan^{-1}(2z/b)]$$

(with one contribution from dispersion and another from focusing) and an amplitude factor $(1+4z^2/b^2)^{(1-q)/2}$ owing to focusing. One expects the harmonic field to be generated in the nonlinear medium through a series of interferences with a period inversely proportional to

$$\Delta k_{\text{eff}}\approx\Delta k_q+2(q-1)/b$$

(at least close to the focus, the period decreases as z increases because of the arctangent term). The expected number of fringes should correspond to the ratio $L/2L_{\text{coh}}$, where the coherence length L_{coh} is $\pi/\Delta k_{\text{eff}}$. Note that L_{coh} becomes progressively shorter for the higher harmonics. However, the number of fringes also depends on how rapidly the amplitude factor $(1+4z^2/b^2)^{(1-q)/2}$ varies throughout the medium. If the amplitude has died away (from the focus) over a length $L_{\text{amp}}\leq L/2$, it is the ratio between this length and L_{coh} that matters for the generation of the harmonic field. In Fig. 11, for $\Delta k_q=0$, in the weak-field limit, we see that the number of oscillations in the harmonic field is 1; this is true for all the harmonics. The field first grows, reaches a maximum value, and then decreases. In this perturbative limit, $L_{\text{amp}}\approx L_{\text{coh}}\ll L/2$, so there is almost perfect matching between the length over which the amplitude is nonnegligible and the coherence length of the process. Consequently, only one oscillation can develop. This leads to almost perfect annihilation of the harmonic field when $L/2\geq L_{\text{amp}}$, as is the case in our example for the harmonics higher than the 5th. This cancellation becomes more efficient as the process order increases, so that the harmonic generation efficiency decreases. We also note in Figs. 11(b), 11(e), 11(c), and 11(f), that the field follows almost exactly the variation of the polarization. Indeed, for the high harmonics, the lower limit of the integral in Eq. (20) can be approximated by $-\infty$ (infinite medium) so that

$$E_q(r,z)\propto(1+2iz/b)^{q-1}\exp[-k_qr^2/(b+2iz)] .$$

The only difference between this and the expression for $P_q(r,z)$ is the exponent of the first term $(1+2iz/b)$ being equal to $q-1$ instead of q. This explains why E_q and P_q are extremely similar for high orders q.

B. Strong-field regime

In the more general situation, the same discussion about the different lengths (L, L_{coh}, and L_{amp}) in the problem applies. In Sec. IV A these lengths have been introduced quite naturally from the expression for the phase-matching integral [Eq. (20)]. In fact, L_{coh} must be interpreted as the length over which the polarization (driving field) and the free Gaussian harmonic field propagating in the medium with the same confocal parameter as the incident beam get out of phase by a factor of π [see Eqs. (13) and (15)]. It is a purely geometric factor, in-

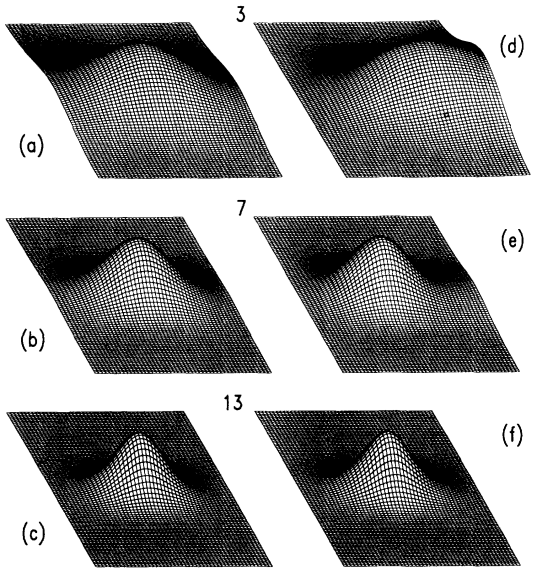

FIG. 11. Graphical representation of $|P_q(r,z)$ (left side) and $|E_q(r,z)|$ (right side) in the nonlinear medium. The light propagates along the horizontal axis (z) from the left to the right. The graphs have been symmetrized around the z axis. The polarization is assumed to be perturbative. From the top to the bottom, the 3rd, 7th, and 13th harmonics have been represented.

dependent of how the dipole moment d_q varies with the laser intensity, whether it is perturbative or not. In contrast, L_{amp}, which represents half the length over which the polarization is nonnegligible, strongly depends on the interaction regime, since the variation of d_q with intensity (and henceforth with z) will be quite different in weak- and in strong-field situations.

To illustrate the essence of the propagation effects in the strong-field regime, we consider a simple model: The polarization is assumed to follow a simple $|E_1|^p$ power law, with an effective order of nonlinearity $p < q$. Figures 12(a)–12(c) present the 7th, 13th, and 21st harmonics generated in a medium whose polarization varies as the fifth power of the incident field. This is a good approximation to the intensity variation of the plateau harmonics in the calculations discussed here. The amplitude of the polarization varies more slowly in the nonlinear medium than in the perturbative case so that $L_{\text{amp}} \gg L_{\text{coh}}$. Therefore, interferences due to phase-matching effects can develop. Two, three-and-a-half, and five-and-a-half oscillations appear in the propagation of, respectively, the 7th, the 13th, and the 21st harmonics. The end of the medium does not necessarily correspond with a minimum in the interference pattern; the harmonic field intensity that leaves the medium is much larger in this case than in the weak-field limit. In addition to the oscillations on the propagation axis, the harmonic profiles do not remain Gaussian throughout the medium. They develop rings. Figures 12(a)–12(c) exhibit a rather nice, regular wave pattern. Even when the far edge of the medium happens to be at a minimum on axis, the intensity of the field does not drop to zero, thanks to this defocusing effect (the maximum of the profiles being then off axis).

In order to emphasize further the importance of the amplitude variation in high-order harmonic generation in a nonlinear medium, we show in Figs. 12(d) and 12(e) the 13th harmonic generated from a polarization varying as the second and eighth power of the incident field. Figure 12(f) displays the 13th harmonic generated from the same polarization as in Fig. 12(b), but with a positive phase mismatch Δk_q (equal to 20 cm^{-1}). By comparing Figs. 12(b), 12(d), and 12(e), one sees how the wave pattern develops depending on the effective order of nonlinearity p. For a very low p, the oscillations are quite pronounced and the profile is strongly deformed compared to its perturbative limit, showing many rings. This is because the amplitude of the polarization extends much farther away from the propagation axis. In contrast, the rings have almost disappeared in Fig. 12(e), though the oscillations on axis remain quite apparent. The variation of the harmonic intensity with the z coordinate is shown in Fig. 13 for several orders of nonlinearity varying from 2 to 13. The vertical scale actually denotes the phase-matching factor, defined as the ratio of the number of photons to the single-atom response. The curve obtained with $p = 2$ has been divided by a factor of 10 in order to be approximately of the same magnitude as the other results. The period of the oscillations is independent of how the polarization varies. However, the efficiency of the process (the phase-matching factor) depends dramatically on the intensity dependence of the polarization amplitude, particularly for very low effective orders of nonlinearity. The less rapidly the polarization varies throughout the medium, the more efficient the generation of the harmonic field. In contrast, a change in the effective phase mismatch only weakly influences the process efficiency. Of course, it can affect the coherence length and the period of the oscillations [compare Figs. 12(b) and 12(f)].

The strength of the harmonic field depends on the length over which it can be built up coherently, L_{coh},

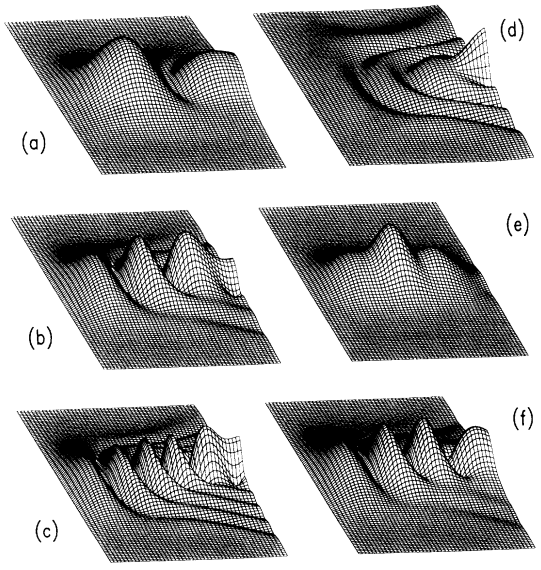

FIG. 12. Graphical representation of $|E_q(r,z)|$ in the nonlinear medium. (a), (b), and (c) show the 7th, 13th, and 21st harmonics calculated by assuming that the polarization varies as the fifth power of the radiation field. (d) and (e) show the 13th harmonic calculated by assuming that the polarization varies as the second and eighth powers of the radiation field. (f) shows the 13th harmonic calculated by assuming that the polarization varies as the fifth power of the radiation field, with a positive phase mismatch equal to 20 cm^{-1}.

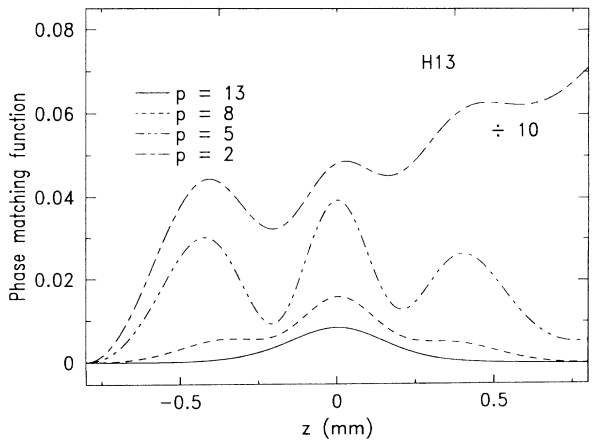

FIG. 13. Phase-matching factor as a function of z for the 13th harmonic. The polarization is assumed to be perturbative (solid line), to follow a second, fifth, or eighth power law.

which is proportional to the laser confocal parameter b when the phase mismatch Δk_q is much smaller than that induced by focusing. Consequently, the intensity of the harmonic field leaving the medium should be approximately proportional to b^2. Since the focal section of the harmonic beam depends on b, this yields a b^3 scaling for the integrated intensity, which has been observed in a series of experiments performed in different focusing conditions [23]. This scaling should be approximately true as long as $L_{\text{coh}} \leq L/2$ and $L_{\text{coh}} \leq L_{\text{amp}}$. In the case of a weakly focused geometry where $L_{\text{coh}} \geq L/2$, the harmonic field does not depend on b, and the integrated intensity (the number of harmonic photons) will vary linearly with the confocal parameter b.

We have tried to understand better the regular wave pattern shown in Fig. 12 by examining the solution of the propagation equation for such model polarization fields (varying as the pth power of the incident field). This solution has been derived in [20] and [25] and can be written as

$$E_q(r',z') = g_q \int_{-L/2}^{z'} G^{q\omega}_{B(z)}(r',z'-Z(z)) \exp[-i\Delta k_q z - iq \tan^{-1}(2z/b) + i \tan^{-1}(2z/b')] \times (1+4z^2/b^2)^{-p/2}(1+4z^2/b'^2)^{1/2} dz \ , \tag{21}$$

where g_q is a constant, $b' = pb/q$,

$$B(z) = b'(b^2+4z^2)/(b'^2+4z^2) \ ,$$

and

$$Z(z) = z(b'^2-b^2)/(b'^2+4z^2) \ .$$

$G^{q\omega}_{B(z)}(r',z'-Z(z))$ is the Gaussian function centered at $z'=Z(z)$ with a confocal parameter equal to $B(z)$. The field that is generated throughout the medium can be interpreted as a sum of Gaussian beams of varying confocal parameters and best-focus positions, which can be either more focused or less focused than in the weak-field limit [$B(z)$ lies between b' and $b''=qb/p$]. Their amplitudes can interfere destructively or constructively depending on the phase term in Eq. (21). This leads to the production of rings in the near- and far-field regions.

On axis ($r'=0$), the integrand in Eq. (21) behaves in a fashion similar to that in Eq. (20), apart from the amplitude term, which varies less rapidly than in the weak-field limit ($p<q$). Off axis ($r' \neq 0$), the Gaussian envelope whose parameters depend on z introduces an additional r'-dependent phase term, equal to

$$2k_q r'^2 (z'-Z(z))/[B(z)^2+4(z'-Z(z))^2] \ .$$

It decreases as z increases, decreasing more rapidly for large r'. Therefore, the coherence length becomes longer away from the beam axis (the period of the spatial oscillations decreases away from axis). This explains the formation of diverging waves as the harmonic field is generated [see Fig. 12(d) in particular] and the defocusing of the harmonic profile.

The previous discussion of the simple model polarization fields is quite general and applies to more complex situations. The key result is that phase matching of the high harmonics depends dramatically on the variation of the amplitude of the polarization field in the medium, and surprisingly weakly on the variation of its phase relative to the fundamental, at least in the conditions studied in the present work. In strong laser fields, the atomic response is nonperturbative and the variation of the harmonic-emission rate with intensity is on average much less rapid than in the weak-field limit. Consequently, the harmonic field gets defocused and phase-matching oscillations can develop over a longer length, so that a significant harmonic intensity gets out of the medium. In contrast, in a weak-field limit, and a tightly focused geometry, the harmonic field created in the first half of the medium gets almost completely canceled out by destructive interference effects in the second half of the medium. One may argue that the conclusions of this section apply only to a tightly focused geometry and will be irrelevant if the laser beam is very weakly focused in the nonlinear medium. This is true for the lower harmonic orders. However, because the coherence length induced by focusing is inversely proportional to the process order q, it will rapidly become smaller than the length of the medium. This means that for very-high-order harmonic-generation processes, the geometry will always become of the tight-focus type.

In this article, we have presented complete *ab initio* calculations of harmonic-generation processes in strong laser fields. They involve the solution of the Schrödinger equation for the outer shell of a rare-gas atom (xenon) and subsequently the integration of the propagation equations for the fundamental and harmonic fields in the paraxial and slowly-varying-envelope approximations. This approach is quite general and allows us to take into account a number of physical effects expected to influence the macroscopic response of a medium exposed to an intense laser field: the nonperturbative response of the atom, the effect of focusing, the linear dispersion and absorption of the atomic medium at the harmonic frequencies, the depletion of the medium owing to ionization, and the influence of the free electrons on the propagation of the fundamental field and on the phase matching of the high harmonics. It does not include, however, wave-mixing processes, nor does it account for rapidly varying phenomena that might become important for very short laser pulses.

The numerical results agree well with experimental data obtained in xenon using a 36-ps-pulse-width 1064-nm-wavelength Nd:YAG laser. We think this approach

might be reliably used for describing other experimental situations (e.g., generation of harmonics of more powerful laser beams focused in different atomic media) and also for making predictions about the specifications that such an extreme ultraviolet source might achieve. Finally, a detailed analysis of how the harmonic fields build up in the medium has provided us with a better understanding of why high harmonics created in a strong-field regime can be efficiently phase matched.

ACKNOWLEDGMENTS

This work has been carried out in part under the auspices of the U.S. Department of Energy at the Lawrence Livermore National Laboratory under contract number W-7405-ENG-48. The Laboratoire d'Energétique Moléculaire et Macroscopique, Combustion (E.M2.C) is "Unité Propre de Recherches No. 288 du CNRS."

[1] K. C. Kulander and B. W. Shore, Phys. Rev. Lett. **62**, 524 (1989); J. Opt. Soc. Am. B **7**, 502 (1990).
[2] J. L. Krause, K. J. Schafer, and K. C. Kulander, Phys. Rev. A **45**, 4998 (1992).
[3] P. L. De Vries, J. Opt. Soc. Am. B **7**, 517 (1990).
[4] K. J. LaGattuta, Phys. Rev. A **41**, 5110 (1990).
[5] R. M. Potvliege and R. Shakeshaft, Phys. Rev. A **40**, 3061 (1989).
[6] J. H. Eberly, Q. Su, and J. Javanainen, Phys. Rev. Lett. **62**, 881 (1989); J. Opt. Soc. Am. B **6**, 1289 (1989).
[7] G. Bandarage, A. Maquet, and J. Cooper, Phys. Rev. A **41**, 1744 (1990).
[8] W. Becker, S. Long, and J. K. McIver, Phys. Rev. A **41**, 4112 (1990).
[9] B. Sundaram and P. W. Milonni, Phys. Rev. A **41**, 6571 (1990).
[10] R. A. Sacks and A. Szöke, J. Opt. Soc. Am. B **8**, 1987 (1991).
[11] V. C. Reed and K. Burnett, Phys. Rev. A **43**, 6217 (1991).
[12] J. Reintjes, *Nonlinear Optical Parametric Processes in Liquids and Gases* (Academic, New York, 1984).
[13] J. F. Ward and G. H. C. New, Phys. Rev. A **185**, 57 (1969).
[14] R. B. Miles and S. E. Harris, IEEE J. Quantum Electron. **QE-9**, 470 (1973).
[15] A. T. Georges, P. Lambropoulos, and J. H. Marburger, Phys. Rev. A. **15**, 300 (1977).
[16] H. Puell, K. Spanner, W. Falkenstein, W. Kaiser, and C. R. Vidal, Phys. Rev. A **14**, 2240 (1978).
[17] A. McPherson, G. Gibson, H. Jara, U. Johann, T. S. Luk, I. McIntyre, K. Boyer, and C. K. Rhodes, J. Opt. Soc. Am. B **4**, 595 (1987).
[18] X. F. Li, A. L'Huillier, M. Ferray, L. A. Lompré, G. Mainfray, and C. Manus, Phys. Rev. A **39**, 5751 (1989).
[19] N. Sarakura, K. Hata, T. Adachi, R. Nodomi, M. Watanabe, and S. Watanabe, Phys. Rev. A **43**, 1669 (1991).
[20] A. L'Huillier, L. A. Lompré, G. Mainfray, and C. Manus, in *Atoms in Intense Laser Fields,* edited by M. Gavrila, Advances in Atomic, Molecular and Optical Physics, Supplement 1 (Academic, New York, in press).
[21] S. W. Allendorf, J. S. Crane, K. S. Budil, and M. D. Perry (unpublished).
[22] A. L'Huillier, P. Balcou, and L. A. Lompré, Phys. Rev. Lett. **68**, 166 (1992).
[23] L. A. Lompré, A. L'Huillier, M. Ferray, P. Monot, G. Mainfray, and C. Manus, J. Opt. Soc. Am. B **7**, 754 (1990).
[24] A. L'Huillier, K. J. Schafer, and K. C. Kulander, Phys. Rev. Lett. **66**, 2200 (1991).
[25] A. L'Huillier, K. J. Schafer, and K. C. Kulander, J. Phys. B **24**, 3315 (1991).
[26] B. W. Shore and K. C. Kulander, J. Mod. Opt. **36**, 857 (1989).
[27] K. C. Kulander and T. N. Rescigno, Comput. Phys. Commun. **63**, 523 (1991); K. C. Kulander, K. J. Schafer, and J. L . Krause, in *Atoms in Intense Radiation Fields* (Ref. [20]).
[28] K. C. Kulander, Phys. Rev. A **38**, 778 (1988).
[29] See, e.g., A. F. Starace *Corpuscles and Radiation in Matter I,* edited by W. Melhorn, Handbuch der Physik Vol. 31 (Springer-Verlag, Berlin, 1982), p. 1.
[30] A. L'Huillier, X. F. Li, and L. A. Lompré, J. Opt. Soc. Am. B **7**, 527 (1990).
[31] T. Auguste, P. Monot, L.-A. Lompré, G. Mainfray, and C. Manus, Opt. Commun. **89**, 145 (1992).
[32] M. C. Downer, W. M. Wood, and J. L. Trisnadi, Phys. Rev. Lett. **65**, 2832 (1990); S. C. Rae and K. H. Burnett, *Proceedings on Short-Wavelength Coherent Radiation,* edited by P. H. Bucksbaum and N. M. Ceglio (Optical Society of America, Washington, DC, 1991), Vol. 11.
[33] A. E. Siegman, *Lasers* (University Science, Mill Valley, CA, 1986).
[34] M. E. Faldon, M. H. R. Hutchinson, J. P. Marangos, J. E. Muffett, R. A. Smith, J. W. G. Tisch, and C. G. Wahlström, J. Opt. Soc. Am. B (to be published).
[35] Blueshifts of the fundamental and of the harmonics have been recently observed by a group at Stanfod University [J. J. Macklin, J. D. Kmetec, G. L. Gordon III, and S. E. Harris, (private communication)]. They also report observation of extremely high-order harmonics (up to the 109th) of an intense femtosecond Ti:Sapphire laser.
[36] A. L'Huillier, P. Balcou, K. J. Schafer, and K. C. Kulander, *Coherence Phenomena in Atoms and Molecules,* edited by A. D. Bandrauk and A. C. Wallace, Proceedings of the NATO workshop (Plenum, New York, in press).

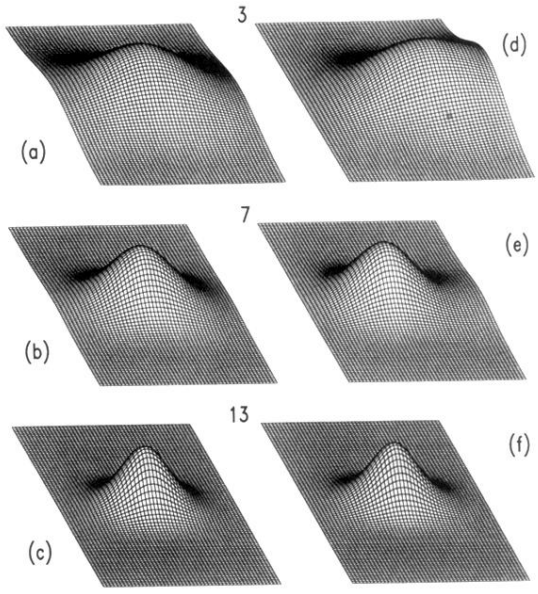

FIG. 11. Graphical representation of $|P_q(r,z)$ (left side) and $|E_q(r,z)|$ (right side) in the nonlinear medium. The light propagates along the horizontal axis (z) from the left to the right. The graphs have been symmetrized around the z axis. The polarization is assumed to be perturbative. From the top to the bottom, the 3rd, 7th, and 13th harmonics have been represented.

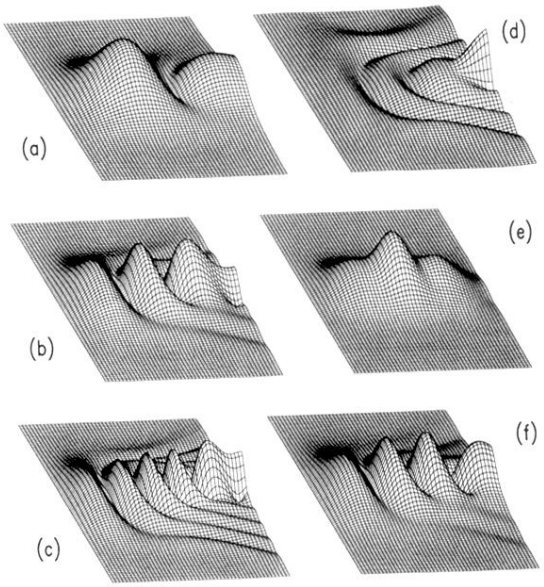

FIG. 12. Graphical representation of $|E_q(r,z)|$ in the nonlinear medium. (a), (b), and (c) show the 7th, 13th, and 21st harmonics calculated by assuming that the polarization varies as the fifth power of the radiation field. (d) and (e) show the 13th harmonic calculated by assuming that the polarization varies as the second and eighth powers of the radiation field. (f) shows the 13th harmonic calculated by assuming that the polarization varies as the fifth power of the radiation field, with a positive phase mismatch equal to 20 cm^{-1}.